DØ Note 5726-CONF

Search for neutral Higgs bosons in multi-b-jet events in $p\bar{p}$ collisions at $\sqrt{s} = 1.96$ TeV

The DØ Collaboration
URL http://www-d0.fnal.gov
(Dated: July 31, 2008)

Data recorded by the D0 experiment during the RunIIb data taking period (June 2006-March 2008) at the Fermilab Tevatron Collider are analyzed to search for neutral Higgs bosons produced in association with b quarks. This production mode can be enhanced in the minimal supersymmetric standard model (MSSM). The search is performed in the three b quark channel using multijet triggered events corresponding to an integrated luminosity of 1.6 fb^{-1}. No statistically significant excess of events with respect to the predicted background is observed. Limits are set on the cross section times branching ratio in the mass range 90 to 220 GeV/c^2. The result from this search is combined with that from the RunIIa search and combined limits and exclusions in the MSSM parameter space are set.

Preliminary Results for Summer 2008 Conferences

I. INTRODUCTION

Supersymmetry (SUSY) [1] is a popular extension of the standard model (SM) which overcomes the hierarchy problem associated with electroweak symmetry breaking and the Higgs mechanism. In contrast to the SM, where only one Higgs doublet is required to break the SU(2) symmetry, SUSY requires the presence of at least two Higgs doublets. In the MSSM five Higgs bosons remain after electroweak symmetry breaking; three neutral: h, H, and A - denoted as ϕ, and two charged: $H^{\pm}$. At tree level the Higgs sector can be parameterized by $\tan\beta$, the ratio of the two Higgs doublet vacuum expectation values, and m_A, the mass of the pseudo-scalar Higgs boson A.

The Higgs-quark couplings in the MSSM are proportional to their SM counterparts, with the exact factor depending on the type of quark (up- or down-type) and on the type of Higgs boson. For large values of $\tan\beta$ at least two Higgs bosons (either A and h, or A and H) have approximately the same mass and couplings to down-type quarks, which are enhanced by a factor $\tan\beta$ relative to the SM ones, while the couplings to up-type quarks are suppressed. In this large $\tan\beta$ region the three Higgs boson couplings follow the sum rule $g^2_{\mathrm{hbb}} + g^2_{\mathrm{Hbb}} + g^2_{\mathrm{Abb}} \approx 2 \times \tan^2\beta \times g^2_{\mathrm{h_{SM}}}$. In $p\bar{p}$ collisions at $\sqrt{s} = 1.96$ TeV at the Fermilab Tevatron Collider, the production of Higgs bosons associated with bottom quarks (highest mass down-type quark) is therefore, in these cases, enhanced by a factor $2 \times \tan^2\beta$ relative to the SM. Due to the $\tan\beta$ enhancement, the main decay for all these bosons is $\phi \to b\bar{b}$ (the branching fraction, $\mathcal{B}(\phi \to b\bar{b})$, is $\approx 90\%$). The enhanced production and branching ratio make the final state with three b jets an important channel in the search for MSSM Higgs bosons at large $\tan\beta$. At a hadron collider this final state has a large background from multijet production which is poorly modeled by simulation, making the search for this topology very challenging.

MSSM Higgs boson production has been studied at LEP which excluded $m_{h,A} < 93$ GeV/c^2 for all $\tan\beta$ values [2]. CDF [3, 4] and D0 [5–7] have extended the MSSM Higgs boson searches to higher masses for high $\tan\beta$ values. This note focuses on data taken during RunIIb (from June 2006 - March 2008), corresponding to 1.6 fb^{-1} [8]. The combined RunIIa and RunIIb datasets more than double the data used in our previous recent RunIIa result [5]. This analysis follows the methodology used in Ref. [5], but both it, and the combination, use the standard D0 modified frequentist limit setting procedure [9], but calculates the limit based only on the shape, and not the normalization, of the final discriminating variable.

II. TRIGGERS

The D0 detector is described in Ref. [10]. Dedicated triggers for the three trigger levels (L1,L2,L3) designed to select events with at least three jets are used in this analysis. Table I give a detailed list of the trigger conditions at all trigger levels. The trigger has an efficiency of $\sim 53\%$ for a Higgs boson with a mass of 150 GeV when measured relative to events with three offline jets.

Level	Trigger Requirement
L1	JT(3,8,$\|\eta\| < 3.2$)JT(2,15,$\|\eta\| < 2.4$)JT(1,30,$\|\eta\| < 2.4$)
L2	JT(1,30,$\|\eta\| < 2.6$) JT(2,15,$\|\eta\| < 2.6$) JT(3,8,no cut) HT(75,6) MJT(10,10) OR JT(1,30,$\|\eta\| < 2.6$) JT(2,15,$\|\eta\| < 2.6$) JT(3,8,no cut) HT(100,6)
L3	JT(3,15,$\|\eta\| < 3.6$) JT(2,25,$\|\eta\| < 3.6$) $\|z_{\mathrm{PV}}\| < 35$ cm $\mathrm{Prob_b}(0.4)$
Name	JT2_3JT15L_IP_VX

TABLE I: The trigger conditions for the $\phi b\bar{b}$ trigger for the RunIIb data sample. The JT(x,y,$|\eta| <$ z) term corresponds to x jets reconstructed at L1, L2 or L3 with $p_T > y$ GeV/c and $|\eta| <$ z (where η is the pseudorapidity). The HT(x,y) term is used only at L2 and requires that the sum of the transverse momenta of L2 jets with $p_T > y$ GeV/c is above x GeV. The MJT(x,y) term corresponds to a missing transverse energy > x GeV calculated from jets with $E_T >$ y GeV. The $\mathrm{Prob_b}(0.4)$ term is used only at L3 and corresponds to a cut of 0.4 on the probability for the event to not contain a b-quark.

III. MONTE CARLO

Signal samples are simulated for Higgs boson masses from 90-220 GeV/c^2 using the leading order PYTHIA event generator [11] to generate associated production of ϕ and a b quark in the 5-flavor scheme, $gb \to \phi b$. Weights, calculated with MCFM [12], are applied to the signal samples as a function of p_T and η of the leading b jet which is not from the decay of the Higgs boson, to correct the cross section and experimental acceptance to next-to-leading order

(NLO). Multijet background events from the $b\bar{b}$, $b\bar{b}j$, $b\bar{b}jj$, $c\bar{c}$, $c\bar{c}j$, $c\bar{c}jj$, $b\bar{b}c\bar{c}$, and $b\bar{b}b\bar{b}$ processes (where j denotes a light parton: u, d, s quark or gluon) are generated with the ALPGEN [13] event generator. The contributions from other processes, such as $t\bar{t}$, $Zb\bar{b}$, and single top production, are negligible. The ALPGEN samples are processed through PYTHIA for showering and hadronization. All samples are then processed through a GEANT-based [14] simulation of the D0 detector and the same reconstruction algorithms as the data. A parameterized trigger simulation is used to model the effects of the trigger requirements on the simulated events.

IV. EVENT SELECTION

Jets are reconstructed from energy deposits in calorimeter towers using the midpoint cone algorithm [15] with radius = 0.5. Jet reconstruction and energy scale determination are described in detail in Ref. [16]. All calorimeter jets are required to pass a set of quality criteria with about 98% efficiency and have at least two reconstructed tracks within $\Delta\mathcal{R}(\text{track, jet-axis}) = \sqrt{(\Delta\eta)^2 + (\Delta\varphi)^2} < 0.5$ (where η is the pseudorapidity and φ the azimuthal angle).

A subset of events is initially selected from the full dataset by requiring a very loose pre-selection requirement of 3 jets with $p_T > 20$, 15 and 15 GeV before jet energy scale corrections have been applied. We select signal events by requiring at least three and at most five jets with $p_T > 20$ GeV/c and $|\eta| < 2.5$ in events with a primary vertex z position within 35 cm of the center of the detector. A neural network (NN) based b-tagging algorithm [17], with lifetime based information involving the track impact parameters and secondary vertices as inputs, is used to identify b jets. Each event must have at least three jets satisfying a tight b-tag NN requirement. The single jet b-tagging efficiency is $\approx 50\%$ for a light-jet mistag rate of $\approx 0.4\%$. The events with at least two tight b tags are also kept and used to model the background. Simulated events are weighted based on their tagging and fake rate probabilities determined from data. Finally, the transverse momenta of the two highest p_T jets which are also b-tagged are required to be above 25 GeV/c. To further increase the sensitivity, the analysis is split into separate three-, four-, and five-jet channels. After the event selection 4,668 events remain in the exclusive three-jet sample, 3,387 and 848 events, respectively, in the four- and five-jet samples. Table II shows the number of events in data at different levels of the event selection.

	Number of events	Fraction relative to previous level
Events	121,457,747	-
Pass trigger	51,973,882	0.428
Pass z vertex cut	51,690,017	0.995
3/4/5 good jets	26,606,009/6,558,214/876,572	0.515/0.127/0.017
2 NN tight b-tag jets ($p_T > 25\,\text{GeV}/c$)	211,177/72,127/12,473	0.008/0.011/0.014
3 NN tight b-tag jets	4,668/3,387/848	0.022/0.047/0.068

TABLE II: The number of events and relative fraction of events in data passing each cut. As we later split the data into 3-, 4- and 5 jet sub-samples, these numbers are reported separately in the last three rows.

A. Signal efficiency

The signal efficiencies after the trigger, z vertex and 3-5 good jet selection for Higgs boson masses between 100 and 200 GeV/c^2 range from 2.5-16.9%. After the complete selection the efficiency ranges from $0.2 - 1.0\%$ in the three-jet channel ($0.1 - 0.4\%$ and $0.02 - 0.08\%$ in the four- and five-jet channels).

V. BACKGROUND COMPOSITION

The background composition is determined from the 3-jet sample. The fractional contribution α_i of the ith background process is calculated from equations linking the b-tag efficiency, ϵ_j, in an event with the N_j observed events:

$$\begin{aligned} \textstyle\sum_i \alpha_i &= 1 \\ \textstyle\sum_i \alpha_i \times \epsilon_j^i &= N_j/N_{\text{tot}} \end{aligned} \tag{1}$$

Here, j indicates the number of b-tagged jets (1-3) in an event for different b-tag criteria, and $N_{\rm tot}$ is the total number of events. The double b-tagged sample is found to be dominated by $b\bar{b}j$ while the triple b-tagged sample consists of a mix of $\approx 50\%$ $b\bar{b}b$, $\approx 35\%$ $b\bar{b}j$, and $\approx 15\%$ $b\bar{b}c + bc\bar{c}$.

VI. ANALYSIS

For every event the two jet pairs with the largest summed transverse momenta are considered as possible Higgs boson candidates. To remove discrepancies between data and simulation originating from gluon splitting ($g \to b\bar{b}$), only jet pairs with $\Delta\mathcal{R} > 1.0$ are considered in the final analysis.

A. Likelihood Discriminant

The following six variables separate the Higgs boson jet pair from the background jet pairs and are well modeled by the simulation: the difference in pseudorapidity between the two jets in the pair; the azimuthal angular difference between the two jets in the pair; the angle between the leading jet in the pair and the total momentum of the pair; $|p_{b_1} - p_{b_2}|/|p_{b_1} + p_{b_2}|$, the momentum balance in the pair; the combined rapidity of the jet pair; and the event sphericity. Based on these kinematic variables, a likelihood discriminant $\mathcal{D}$, is calculated according to:

$$\mathcal{D}(x_1, ..., x_6) = \frac{\prod_{i=1}^{6} P_i^{sig}(x_i)}{\prod_{i=1}^{6} P_i^{sig}(x_i) + \prod_{i=1}^{6} P_i^{bkg}(x_i)}, \tag{2}$$

where P_i^{sig} (P_i^{bkg}) refers to the signal (background) probability density function (pdf) for variable x_i, and $(x_1, ..., x_6)$ is the set of measured kinematic variables for the jet pair. The pdfs are obtained from triple b-tagged signal and background simulation. Two likelihoods are built combining simulated samples in the $90 - 130\,\mathrm{GeV}/c^2$ ("low-mass") and $130 - 220\,\mathrm{GeV}/c^2$ ("high-mass") mass ranges, providing discrimination at low and high masses, respectively.

B. Background Estimation

Several multijet processes contribute to the background and the uncertainty on their cross sections is large. The bbb component may also contain a contribution that is indistinguishable from a signal and cannot be normalized from the data. To model the background we therefore rely on a combination of data and simulation. The distribution of the expected triple b-tagged (3Tag) sample in the two-dimensional $\mathcal{D}$ and invariant mass (M_{bb}) plane, $S^{exp}_{\rm 3Tag}(\mathcal{D}, M_{bb})$, is obtained from the double b-tagged (2Tag) data shape multiplied by the ratio of the simulated (MC) shapes of the triple and double tagged events:

$$S^{exp}_{\rm 3Tag}(\mathcal{D}, M_{bb}) = \frac{S^{MC}_{\rm 3Tag}(\mathcal{D}, M_{bb})}{S^{MC}_{\rm 2Tag}(\mathcal{D}, M_{bb})} S^{data}_{\rm 2Tag}(\mathcal{D}, M_{bb}). \tag{3}$$

Many uncertainties affecting the simulation cancel in the ratio $\frac{S^{MC}_{\rm 3Tag}(\mathcal{D}, M_{bb})}{S^{MC}_{\rm 2Tag}(\mathcal{D}, M_{bb})}$. Figure 1 shows $\mathcal{D}$ for data and background for the low- and high-mass likelihood in the three-jet channel.

The selection cuts on $\mathcal{D}$, b-tagging, and number of jet-pair combinations per event were optimized by maximizing the expected sensitivity for the analysis in [5]. The optimal cuts for the likelihood were found to vary between 0.25 and 0.60 depending on the jet multiplicity and Higgs boson mass. The likelihood and other optimisations were retained unchanged in this analysis. Figure 2 shows the invariant mass for the optimized high-mass likelihood cuts, Figure 3 for the low-mass likelihood.

C. Systematic Uncertainties

Sources of systematic uncertainty on the signal acceptance and background shape are considered. The signal systematics were retained from [5], whilst those effecting the background again dominate and were re-derived. The sources of signal systematic included are: integrated luminosity, theoretical, trigger efficiency, jet identification, jet

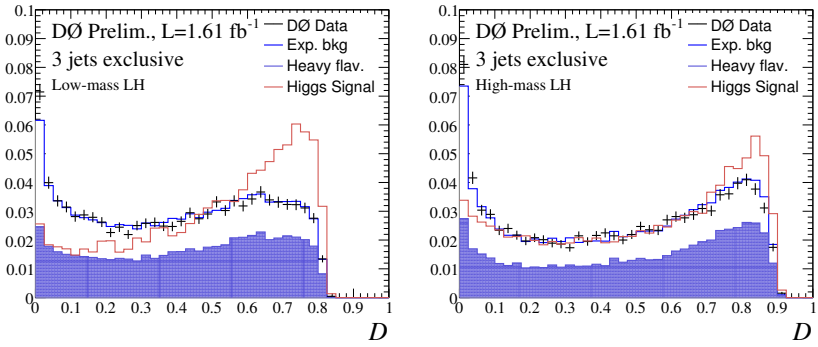

FIG. 1: Comparison of the low- and high-mass likelihood distributions for the 3Tag data and background (bkg exp.) defined by Eq. 3. Every event has two entries, one for each jet pair. Black crosses refer to data, the solid blue line shows the total background estimate, and the dotted green represents the heavy flavor component ($b\bar{b}b$, $b\bar{b}c$, and $c\bar{c}b$). The distributions for a Higgs boson of mass 100 and 180 GeV/c^2 are also shown.

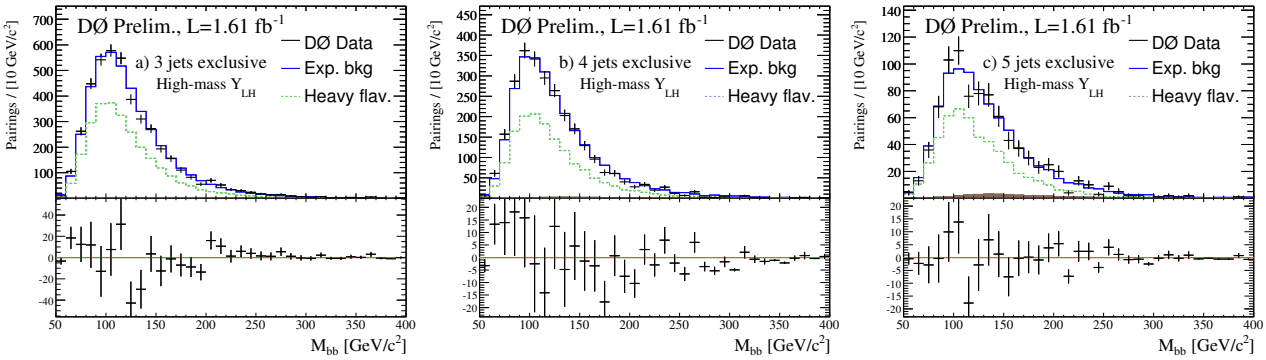

FIG. 2: Invariant mass for the high-mass likelihood region for the exclusive a) three-jet b) four-jet, and c) five-jet channels. Black crosses refer to data, the solid blue line shows the total background estimate, and the dotted green line represents the heavy flavor component ($b\bar{b}b$, $b\bar{b}c$, and $c\bar{c}b$). The lower panels show the difference between the data and the background expectation.

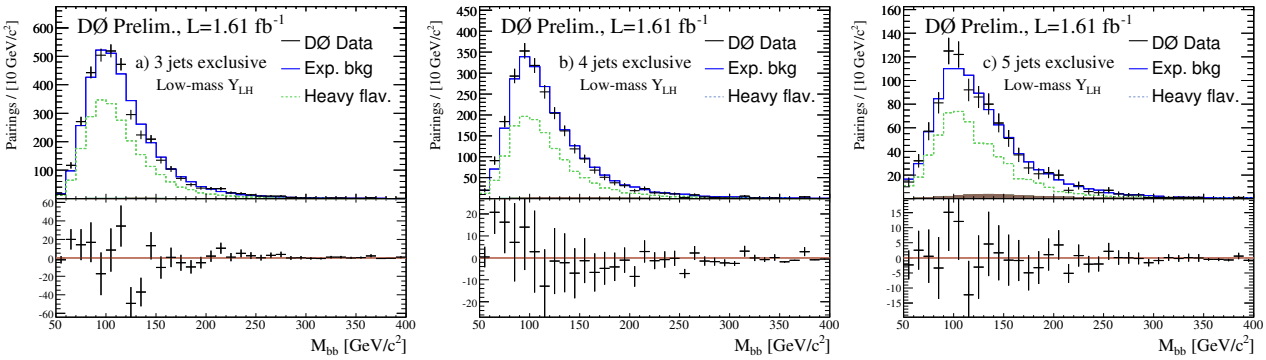

FIG. 3: Invariant mass for the low-mass likelihood region for the exclusive a) three-jet b) four-jet, and c) five-jet channels. Black crosses refer to data, the solid line shows the total background estimate, and the shaded region represents the heavy flavor component ($b\bar{b}b$, $b\bar{b}c$, and $c\bar{c}b$). The lower panels show the difference between the data and the background expectation.

energy calibration, jet energy resolution, and b jet identification. These are added in quadrature, and give a total error of 17 - 18%. For the background, only systematic uncertainties affecting the shape of M_{bb} matter, since only the shape and not the normalization is used to distinguish signal from background in this analysis. Several sources of systematic uncertainties affecting the background shape through the ratio $\frac{S^{MC}_{3\mathrm{Tag}}(\mathcal{D},M_{bb})}{S^{MC}_{2\mathrm{Tag}}(\mathcal{D},M_{bb})}$ in Eq. 3 are parametrized as a function of M_{bb}. The dominant uncertainty, due to the background composition, is estimated by varying the ratio of $b\bar{b}j$ and $b\bar{b}b$ events in the sample corresponding to the uncertainties from the background composition fit ($\approx 20\%$). The uncertainty from the kinematic dependence of the b-tagging of jets is evaluated by varying the b and c jet tag efficiencies within their uncertainties. The uncertainty from the b-jet energy resolution is obtained by smearing the b and c jets by an additional 7%. Uncertainties in the modelling of the $b\bar{b}j$ kinematics are assessed making use of a control data sample. A comparison of the $\frac{S_{3\mathrm{Tag}}(M_{bb})}{S_{2\mathrm{Tag}}(M_{bb})}$ in Monte Carlo and a data sample both selected in the low $\mathcal{D}$ region is used to estimate additional uncertainties on the background model. Finally, the small shape difference between triple and double b-tagged data in the turn-on of the trigger level b-tag is accounted for as a systematic uncertainty.

VII. RESULTS

The modified frequentist, or CL_s, method [9, 18] is used to calculate limits, using only the shapes (not the normalization) of the M_{bb} distributions to discriminate signal from background. The confidence level, CL_s, is defined as $CL_s = CL_{s+b}/CL_b$, where CL_{s+b} and CL_b are the confidence levels in the signal-plus-background and background-only hypotheses. The systematic uncertainties on the signal and background shapes are included in the limit setting procedure using Gaussian prior probability densities. Limits on $\sigma \times \mathrm{Br}$ are obtained by scaling the signal cross section until $1-CL_s = 0.95$ is reached. In the simple enhancement scenario the width of ϕ is assumed to be negligible relative to the experimental resolution ($\approx 20\%$) and the cross section $\times$ branching ratio is taken to be $2 \times \tan^2\beta \times (\sigma \times \mathrm{Br})_{SM}$. Figures 4 and 5 shows the observed and expected (with $\pm$ 1 and 2 σ uncertainties as the yellow and green bands respectively) 95% confidence level exclusion limits for this analysis and the combined RunIIa [5] and RunIIb analyses respectively. These results are summarized numerically in Tables III and IV.

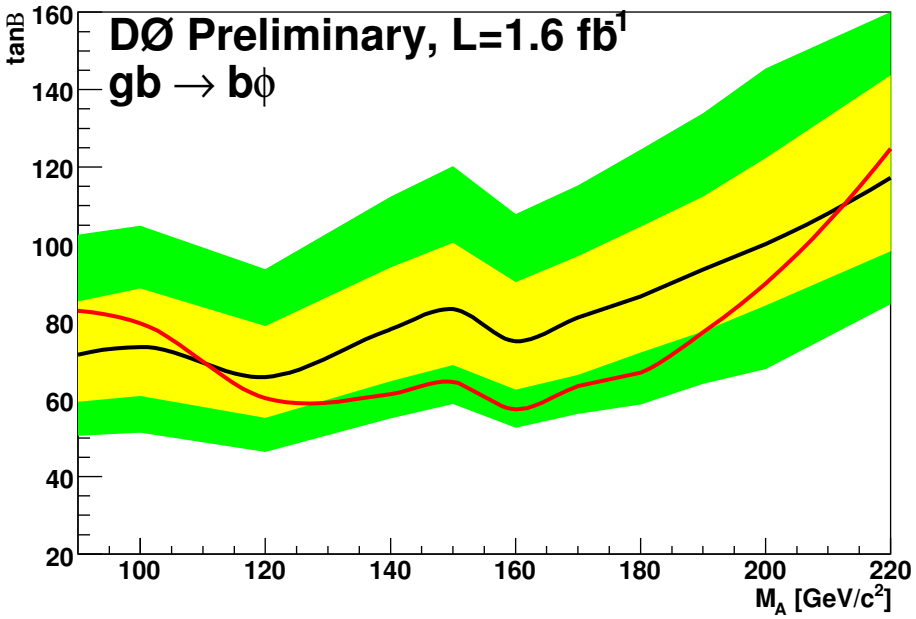

FIG. 4: 95% CL exclusion limit in the $(m_A, \tan\beta)$ plane using the simple enhancement $2 \times \tan\beta^2 \times (\sigma \times \mathrm{Br})_{SM}$ for the RunIIb analysis. The red curve is the observed limit. The black curve is the expected limit (in the no-signal hypothesis) and the bands correspond to $\pm 1\sigma$ and $\pm 2\sigma$ variations around the expectation.

As a consequence of the enhanced couplings to b quarks at large $\tan\beta$ the total width of the neutral Higgs bosons also increases with $\tan\beta$. This can have an impact on our search if the width is comparable to or larger than the

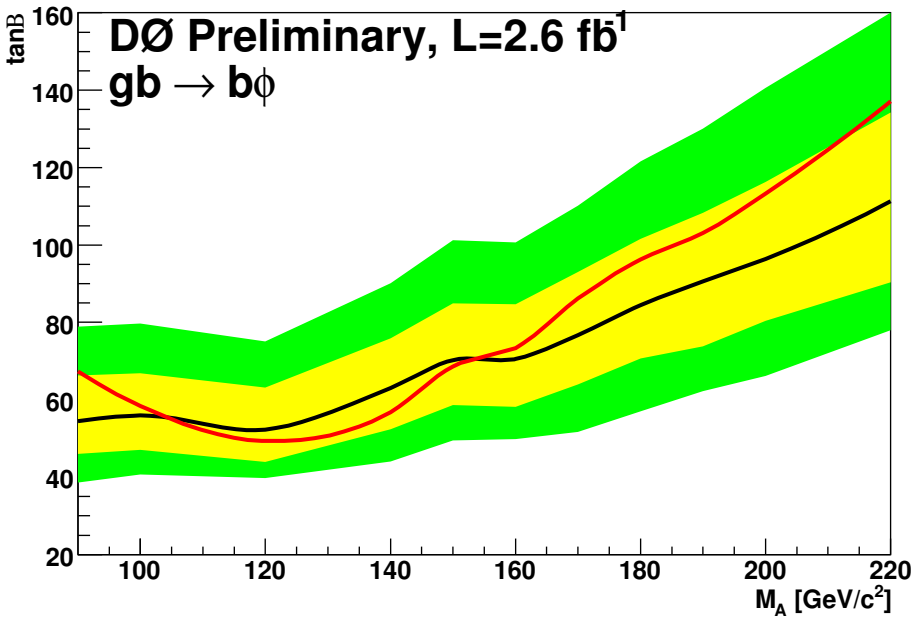

FIG. 5: 95% CL exclusion limit in the $(m_A, \tan\beta)$ plane using the simple enhancement $2 \times \tan\beta^2 \times (\sigma \times \mathrm{Br})_{SM}$ for the combination of the current and RunIIa [5] analyses. The red curve is the observed limit. The black curve is the expected limit (in the no-signal hypothesis) and the bands correspond to $\pm 1\sigma$ and $\pm 2\sigma$ variations around the expectation.

m_A/GeV/c^2	Tanβ Obs.	Tanβ Exp.	$\sigma\times$Br. Obs./pb	$\sigma\times$Br. Exp./pb
90	83	71^{+14}_{-12}	200.7	$149.1^{+63.2}_{-46.3}$
100	80	73^{+15}_{-13}	121.7	$103.8^{+47.0}_{-32.6}$
110	68	70^{+14}_{-12}	58.9	$64.2^{+28.1}_{-20.6}$
120	60	66^{+13}_{-11}	32.7	$38.9^{+17.1}_{-11.5}$
130	50	71^{+13}_{-13}	15.8	$31.4^{+12.7}_{-10.6}$
140	61	78^{+16}_{-13}	16.9	$27.4^{+12.4}_{-8.6}$
150	64	83^{+17}_{-14}	13.6	$22.6^{+10.3}_{-7.1}$
160	57	75^{+15}_{-13}	7.9	$13.5^{+6.0}_{-4.1}$
170	63	81^{+16}_{-15}	7.1	$11.6^{+5.0}_{-3.9}$
180	67	87^{+18}_{-15}	5.9	$9.9^{+4.6}_{-3.1}$
190	77	93^{+19}_{-16}	6.0	$8.8^{+3.9}_{-2.8}$
200	90	100^{+22}_{-16}	6.2	$7.7^{+3.7}_{-2.2}$
210	107	109^{+23}_{-19}	6.7	$7.1^{+3.3}_{-2.2}$
220	125	117^{+27}_{-19}	7.2	$6.3^{+3.2}_{-1.9}$

TABLE III: Observed and expected 95% C.L. limits in Tanβ and cross section times branching ratio for the 1.6fb^{-1} analysis in the negligible width scenario.

experimental resolution of the reconstructed invariant mass of the di-jet system. To take this effect into account, the width of the Higgs boson is calculated with FEYNHIGGS [19] and included in the simulation as a function of the mass and $\tan\beta$ by convoluting a relativistic Breit-Wigner function with the NLO cross section. In the MSSM the masses and couplings of the Higgs bosons depend, in addition to $\tan\beta$ and m_A, on the SUSY parameters through radiative corrections. Limits on $\tan\beta$ as a function of m_A are derived for one particular scenario assuming a CP-conserving Higgs sector [20]: the m_h^{max} scenario with a negative value of the Higgs sector bilinear coupling μ. Figure 6 shows the result obtained in the present analysis interpreted in this MSSM scenario. Substantial areas in the MSSM parameter phase space up to masses of 220 GeV/c^2 are excluded. Figure 7 shows the combined result of the present analysis and the RunIIa analysis from Ref.[5]. The expected limit is improved by combining the RunIIa and RunIIb datasets. However the observed limit is more convoluted as it reflects the data excess observed in RunIIa at high masses and

m_A/GeV/c^2	Tanβ Obs.	Tanβ Exp.	$\sigma\times$Br. Obs./pb	$\sigma\times$Br. Exp./pb
90	67	55^{+12}_{-9}	132.4	$86.9^{+41.6}_{-25.0}$
100	58	56^{+11}_{-9}	65.6	$60.1^{+25.7}_{-17.5}$
110	52	54^{+12}_{-8}	35.1	$37.6^{+17.9}_{-10.4}$
120	49	52^{+11}_{-8}	21.9	$24.6^{+11.3}_{-7.3}$
130	44	56^{+11}_{-9}	12.1	$19.6^{+8.8}_{-5.7}$
140	57	63^{+13}_{-11}	14.5	$17.9^{+8.1}_{-5.6}$
150	69	70^{+15}_{-12}	15.4	$16.1^{+7.4}_{-4.9}$
160	73	71^{+14}_{-12}	12.9	$11.9^{+5.2}_{-3.8}$
170	86	77^{+16}_{-13}	13.1	$10.4^{+4.9}_{-3.2}$
180	96	84^{+17}_{-14}	12.3	$9.5^{+4.2}_{-2.8}$
190	103	91^{+18}_{-17}	10.7	$8.3^{+3.5}_{-2.8}$
200	113	96^{+20}_{-16}	9.9	$7.1^{+3.3}_{-2.2}$
210	124	104^{+22}_{-18}	9.1	$6.4^{+2.9}_{-2.0}$
220	137	111^{+23}_{-21}	8.7	$5.7^{+2.6}_{-1.9}$

TABLE IV: Observed and expected 95% C.L. limits in Tanβ and cross section times branching ratio for the 2.6fb^{-1} analysis in the negligible width scenario.

the deficit observed in RunIIb at intermediate masses.

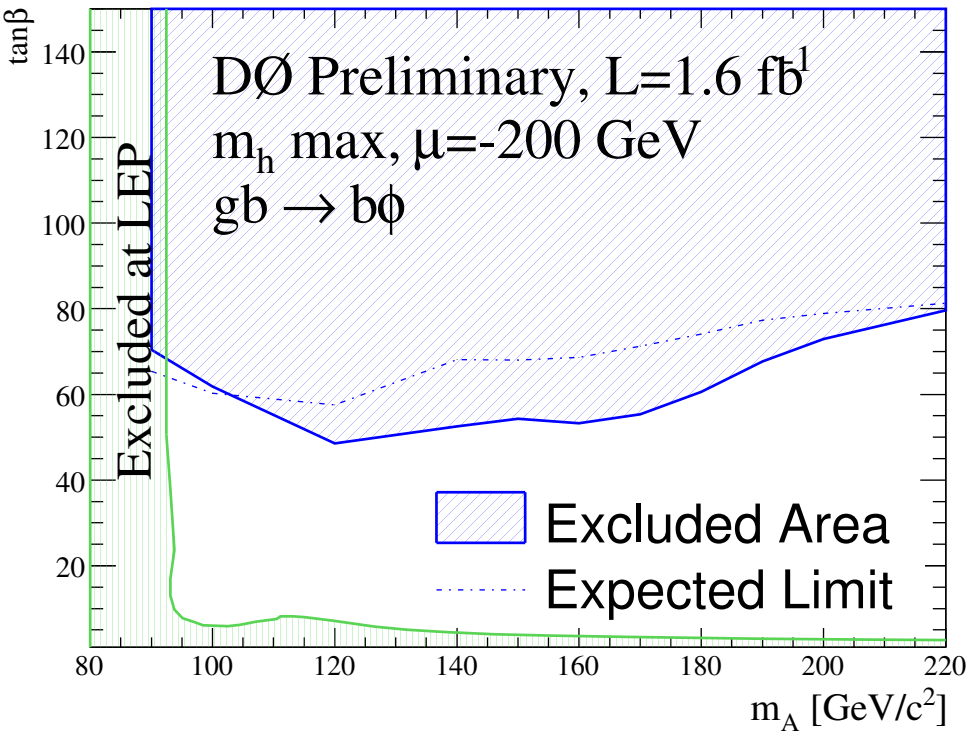

FIG. 6: 95% CL exclusion limit in the $(m_A, \tan\beta)$ plane obtained with the current analysis for the $m_h^{\rm max}$, μ=-200 GeV scenario. The exclusion limit obtained from the LEP experiments is also shown [2].

We thank the staffs at Fermilab and collaborating institutions, and acknowledge support from the DOE and NSF (USA); CEA and CNRS/IN2P3 (France); FASI, Rosatom and RFBR (Russia); CNPq, FAPERJ, FAPESP and FUNDUNESP (Brazil); DAE and DST (India); Colciencias (Colombia); CONACyT (Mexico); KRF and KOSEF (Korea); CONICET and UBACyT (Argentina); FOM (The Netherlands); STFC (United Kingdom); MSMT and GACR (Czech Republic); CRC Program, CFI, NSERC and WestGrid Project (Canada); BMBF and DFG (Germany); SFI (Ireland); The Swedish Research Council (Sweden); CAS and CNSF (China); and the Alexander von Humboldt

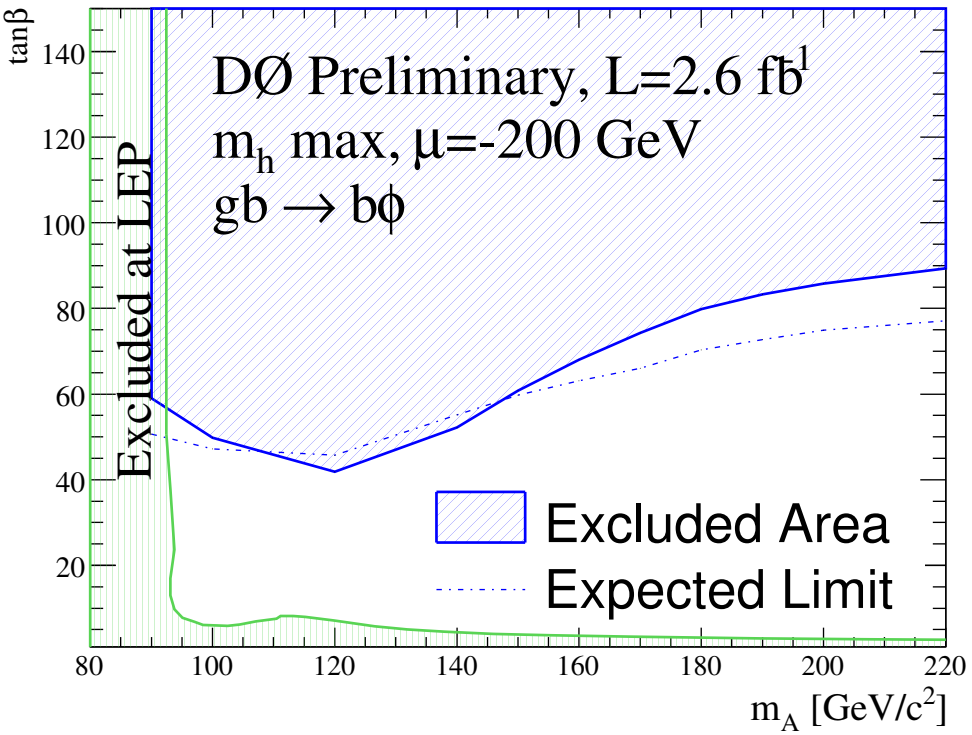

FIG. 7: 95% CL exclusion limit in the $(m_A, \tan\beta)$ plane obtained with the combination of the current and RunIIa [5] analyses for the $m_h^{\rm max}$, μ=-200 GeV scenario. The exclusion limit obtained from the LEP experiments are also shown [2].The width of ϕ is larger than 70% of m_A above $\tan\beta = 100$ in the $m_h^{\rm max}$, $\mu = -200$ GeV scenario.

Foundation (Germany).

[1] H.P. Nilles, Phys. Rep. **110**, 1 (1984); H.E. Haber and G.L. Kane, Phys. Rep. **117**, 75 (1985).
[2] S. Schael *et al.* (The ALEPH, DELPHI, L3, and OPAL Collaborations), Eur. Phys. J. C **47**, 547 (2006).
[3] T. Affolder *et al.* (CDF collaboration), Phys. Rev. Lett. **86**, 4472 (2001).
[4] A. Abulencia *et al.* (CDF Collaboration), Phys. Rev. Lett. **96**, 011802 (2006).
[5] V.M. Abazov *et al.* (D0 Collaboration), arXiv:hep-ex/0805.3556 (2008).
[6] V.M. Abazov *et al.* (D0 Collaboration), Phys. Rev. Lett. **95**, 151801 (2005).
[7] V.M. Abazov *et al.* (D0 Collaboration), arXiv:hep-ex/0805.2491 (2008).
[8] T. Andeen *et al.*, FERMILAB-TM-2365 (2007).
[9] W. Fisher, FERMILAB-TM-2386-E (2007).
[10] V.M. Abazov *et al.* (D0 Collaboration), Nucl. Instrum. Methods Phys. Res. A **565**, 463 (2006).
[11] T. Sjöstrand *et al.*, arXiv:hep-ph/0308153 (2003).
[12] J. Campbell, R.K. Ellis, F. Maltoni, and S. Willenbrock, Phys. Rev. D **67**, 095002 (2003).
[13] M.L. Mangano *et al.*, J. High Energy Phys. **307**, 001 (2003).
[14] R. Brun and F. Carminati, CERN program library long writeup W5013 (1993).
[15] G. Blazey *et al.*, arXiv:hep-ex/0005012 (2000).
[16] V.M. Abazov *et al.* (D0 Collaboration), Fermilab-Pub-08/034-E (2008).
[17] T. Scanlon, FERMILAB-THESIS-2006-43.
[18] T. Junk, Nucl. Instrum. Methods Phys. Res. A **434**, 435 (1999); A. Read, Nucl. Instrum. Methods Phys. Res. A **425**, 357 (1999).
[19] S. Heinemeyer, W. Hollik, and G. Weiglein, Eur. Phys. J. C **9**, 343 (1999); Comput. Phys. Commun. **124**, 76 (2000); G. Degrassi *et al.*, Eur. Phys. J. C **28**, 133 (2003), M. Frank *et al.*, JHEP **0702**, 047 (2007). We used FEYNHIGGS version 2.6.3.
[20] M. Carena, S. Heinemeyer, C. E. M. Wagner, and G. Weiglein, Eur. Phys. J. C **45**, 797 (2006).